Mon. Not. R. Astron. Soc. **318**, 809–816 (2000)

Sputtering of grains in C-type shocks

P. W. May,[1] G. Pineau des Forêts,[2,3] D. R. Flower,[4★] D. Field,[5] N. L. Allan[1] and J. A. Purton[6]

[1]*School of Chemistry, The University, Bristol BS8 1TS*
[2]*DAEC, Observatoire de Paris, F-92195 Meudon Principal Cedex, France*
[3]*Institut d'Astrophysique Spatiale, Université de Paris XI, F-91405 Orsay Cedex, France*
[4]*Physics Department, The University, Durham DH1 3LE*
[5]*Institute of Physics and Astronomy, University of Århus, Ny Munkegade, DK-8000 Århus C, Denmark*
[6]*CLRC, Daresbury Laboratory, Warrington, Cheshire WA4 4AD*

Accepted 2000 June 14. Received 2000 March 13

ABSTRACT

Sputtering yields are reported for the release of Mg, Fe, Si and O under impact of He, C, O, Si and Fe on grain material composed of Mg- and Fe-bearing silicates. The yields were derived using the TRIM code, which simulates the results of the transport of ions in matter by means of classical Monte Carlo techniques. The energetics of the sputtering process are a key factor in the sputtering calculations, and so detailed determinations have been made of the energy with which atoms are bound to the lattice, using solid-state simulation programs. The probability of ejection of an atom is computed at a given energy, for a number of angles of incidence, and integrated to obtain the mean yield at that energy. These numerical results are then fitted with a simple function of energy for convenience in subsequent applications.

A grid of C-type shock models has been computed, using our new sputtering yields, for pre-shock densities in the range $10^4 \leqslant n_{\rm H} = n({\rm H}) + 2n({\rm H_2}) \leqslant 10^6\,{\rm cm^{-3}}$ and shock speeds $20 \leqslant v_{\rm s} \leqslant 45\,{\rm km\,s^{-1}}$. Sputtered fractions can be high, exceeding 50 per cent for shock speeds in excess of approximately $40\,{\rm km\,s^{-1}}$. The column densities of Si and SiO were also computed, for comparison with observations.

Key words: shock waves – ISM: jets and outflows.

1 INTRODUCTION

In an earlier work (Field et al. 1997; hereafter FMFF), sputtering yields were reported for amorphous carbon and amorphous SiO_2 targets, for sputtering of C, Si and O from these targets by impact of He, C, O, Si and Fe. The consequences for the chemistry in C-type shocks were very briefly explored with special reference to the production of gas-phase SiO. Our purpose in the present work is twofold. In the first place, we seek to make available values of sputtering yields for targets that mimic more closely the composition of interstellar grains. To this end, the sputtering of grains composed of Mg- and Fe-bearing silicates is studied here. The results are relevant to the oxygen-rich environments in which outflows, associated with star formation, are typically found. In the second place, the new sputtering data are used in a sophisticated C-type shock model to yield a grid of results for a range of shock parameters, notably the shock velocity, pre-shock gas density and magnetic field. These models determine, for example, the budget of refractory material in the gas phase, in particular of SiO. These results may be used in conjunction with observational data (e.g. Dutrey, Guilloteau & Bachiller 1997; Lefloch et al. 1998) as a guide to the shock conditions in any particular region.

In Section 2 the technical means for calculating sputtering yields are described, with particular reference to the energetics of the processes involved in sputtering. Sputtering yields are presented in Section 3 for magnesium silicate (Mg_2SiO_4), or 'forsterite', iron silicate (Fe_2SiO_4), or 'fayalite' and an 'olivine', $MgFeSiO_4$, for a variety of projectile species. In Section 4, the grid of shock models is presented and brief reference is made to molecular outflows in regions of star formation.

2 CALCULATION OF SPUTTERING YIELDS

FMFF described how the well-known code transport of ions in matter (TRIM; Ziegler Biersack & Littmark 1985) could be used to calculate sputtering yields for interstellar grains. The reader is referred to FMFF for a more detailed account of the operation of TRIM. Further information, describing recent versions of TRIM, may also be found at www.research.ibm.com/ionbeans/SRM/SRMINTR.HTM. To recapitulate briefly, the TRIM code was developed to simulate the effects of ion bombardment of surfaces (see Eckstein 1991). The code operates by following classical

★ E-mail: david.flower@dur.ac.uk (DRF)

trajectories of impacting particles as they enter the surface of the target and undergo a series of binary collisions with the target atoms, losing energy in each successive collision. The trajectories of displaced target atoms are also followed. Back-scattering of the original projectile, implantation into the target, or sputtering of the target material may result. Many trajectories are followed, up to 10^7 being used in the present study, for a specific impact angle and energy. The sputter yield is given directly by the number of sputtered atoms divided by the total number of impacting particles used in the simulation. The limit on the number of trajectories places a lower limit of significance $\approx 10^{-6}$ on the calculated sputter yields.

The target is considered to be an amorphous solid, with target atoms distributed randomly throughout the solid, which has a defined density. Collisions occur at random locations, based upon a particle mean free path, itself dependent upon the nuclear stopping powers of the particle–target-atom collision partners (see Pirronello 1993; Ziegler et al. 1985). A simplifying assumption in TRIM is that the target remains unchanged as far as atom trajectories are concerned for all the trajectories studied and thus no account is taken of any prior implantation, damage or sputtering effects. The version of TRIM used in the present work is SRIM-96 (96.01). This version runs on a PC and uses more accurate stopping powers and cross-sections than the version used in FMFF (Ziegler et al. 1985).

In order to obtain reliable results for sputtering yields using TRIM, considerable care must be employed in defining the energetics of events that lead to sputtering. The computation of the various energies is an important facet of the present work and is discussed here in more detail than in FMFF.

The energies involved in sputtering are: the surface binding energy, E_S; the displacement energy, E_D; the lattice binding energy, E_B; and the cut-off energy, E_C. We deal with three different materials: forsterite, fayalite and an iron–magnesium silicate, that is, an olivine containing equal quantities of Mg and Fe; we refer to this material simply as 'olivine'. We shall now consider the values of the four energies that should be assigned to each of these materials. Note that an ion which is bound at a lattice site is located in a potential well of depth E_B relative to its energy at infinite separation. In order to escape from its site, a recoiling ion must overcome a potential barrier of height E_D, relative to the potential minimum, and loses a net energy E_B on escaping.

2.1 Surface binding energy, E_S

E_S is the energy holding a surface atom to the lattice. An atom passing through the surface layer must have at least this energy to exit the solid and become a sputtered particle. For a multi-component target, we assume that there is an average surface energy relevant to all atoms equally. E_S may be considered as an energy barrier arising from a plane parallel potential acting to prevent particles leaving the solid. The heat of atomization of a solid may be used as an estimate for E_S. The example of fayalite illustrates this point. Using the JANAF tables, we find

$$Fe_2SiO_4(s) \rightarrow Fe(s) + 2O_2(g) + Si(s)\Delta H^{\ominus} = 1479.9\,kJ\,mol^{-1}$$

$$Si(s) \rightarrow Si(g)\Delta H^{\ominus} = 450\,kJ\,mol^{-1}$$

$$2O_2(g) \rightarrow 4O(g)\Delta H^{\dagger} = 988\,kJ\,mol^{-1}$$

$$Fe_2(s) \rightarrow 2Fe(g)\Delta H^{\ominus} = 809\,kJ\,mol^{-1}$$

yielding a heat of atomization of $3726.4\,kJ\,mol^{-1}$. Thus the average heat of atomization is $532.3\,kJ\,mol^{-1}$ or $5.52\,eV\,atom^{-1}$. Similar calculations for forsterite yield a heat of atomization of 5.60 eV and, for olivine, 5.64 eV. FMFF had not appreciated that E_S could be evaluated reliably in this manner and the present estimates remove a significant degree of uncertainty in our computations.

2.2 Displacement energy, E_D

The displacement energy E_D may be described as follows. An ion in the solid is bound in a potential of some characteristic depth. When this ion is struck by another particle, it will oscillate within this potential but will not be able to escape from its lattice site unless it has been given an additional energy which is at least equal to the displacement energy. Very few reliable data are available in the literature for displacement energies of silicates or related ceramics and oxides. The best estimates (Hayes & Stoneham 1985; Lidiard, personal communication) for displacing Mg and O in MgO are 52 and 54 eV, respectively, and for displacing Al and O in Al_2O_3 are 18 and 75 eV, respectively. For lack of better information, we have taken the values for MgO as a guide, using $E_D = 50$ eV for every type of atom in all three compounds.

2.3 Lattice binding energy, E_B

A major effort has been made to calculate E_B, the energy that binds an atom to a lattice site. A recoiling lattice atom loses this energy before it encounters any other target atom. An approximate figure of 3 eV was used in FMFF. E_B is, however, an important parameter for estimating sputtering yields, as demonstrated in FMFF. For example, results in FMFF show that the position of the sputtering threshold varied by between 5 and $10\,km\,s^{-1}$ for He^+ sputtering Si from SiO_2 or C from amorphous carbon, when E_B was varied between 0 and 3 eV. The value of E_B is given, approximately, by the vacancy energy less the sum of the ionization potentials of the ion in question. The vacancy energy is defined as the energy required to remove the ion from the lattice to infinity, allowing the lattice to relax around the empty site. Vacancy energies for the various ionic species in the different lattices were obtained using a modern solid-state simulation program described below.

Calculations were performed within the framework of an ionic model in which integral ionic charges are assigned to the component atoms, based on accepted chemical valence and electron counting, i.e. 2+ for Mg and Fe, 4+ for Si and 2- for O. The shell model of Dick & Overhauser (1958) is used to take account of electronic polarization. Simulations of the perfect lattice yield the crystal structure and the corresponding lattice energy. In the static limit, the structure is determined by the condition $\partial E/\partial X_i = 0$, where E is the static contribution to the internal energy, and the X_i are the variables that define the structure. These are the three lattice vectors, the atomic positions in the unit cell and, in the case of the shell model, the shell displacements (Taylor et al. 1997). The most convenient approach to vacancy and other defect energies is the two-region approach introduced by Lidiard & Norgett (1972) and described in full by Catlow & Mackrodt (1982). In this method, the total energy of the defective system is minimized by a relaxation of the nuclear positions and shell displacements of the ions surrounding the defect. It is a reasonable assumption that this relaxation is greatest in the proximity of the defect and that the relaxations decrease fairly rapidly with distance from the defect. The crystal is accordingly partitioned into an inner region immediately

Table 1. Values of vacancy energies and lattice binding energies calculated using the method outlined in the text. Ionization potentials for the positive ions are the values required to form the appropriate multiply charged ion. For lattice oxygen, we have used values of −9.2 and 0.2 eV for the first and second ionization potentials of O^{2-}, calculated using the methods of Mackrodt & Stewart (1979). The value for the first ionization energy is close to that (−9.0 eV) suggested by Dickens, Heckingbottom & Linnett (1968) to account for the values of the heat of formation of a wide range of oxides.

Species observed	Vacancy energy (eV)	Ionization potential (eV)	Lattice binding energy (eV)
Mg^{2+}	24.5	22.6	1.9
Si^{4+}	107.1	103.1	4.0
O^{2-}	24.5	9.0	15.5
Fe^{2+}	23.6	24.1	≈0

surrounding the defect, where the relaxations are assumed to be greatest, and an outer region which is only slightly perturbed. In the inner region, the appropriate elastic equations for the force are solved explicitly, yielding the relaxed nuclear positions and shell displacements. In the outer region, however, the latter are estimated using a suitable approximation, in this case that suggested by Mott & Littleton (1938). The success of any simulation relies on the accuracy and transferability of the short-range interatomic potentials. We have used a well-established set of potentials based on the transferability of potentials from SiO_2 (Sanders, Leslie & Catlow 1984) and binary oxides such as MgO and FeO (Lewis & Catlow 1985). The model has been demonstrated to reproduce accurately the structure and thermodynamic properties of a wide range of minerals (e.g. Patel, Price & Mendelssohn 1991; Winkler, Dove & Leslie 1991; Purton, Allan & Blundy 1997a), including olivine and also the partitioning of trace elements between coexisting silicate phases (Purton et al. 1996; Purton, Allan & Blundy 1997b).

Vacancy energies of the various species, ionization potentials and resulting lattice binding energies are shown in Table 1. Vacancy energies in the environments of the three different compounds were found to be negligibly different and a single value is quoted for each species. The uncertainty to be assigned to the resulting lattice binding energies in Table 1 is ±0.5 eV. Since TRIM is able to handle only a single value of E_B for each compound, a weighted average of the values of E_B in Table 1 has been used in each case. Thus for fayalite, a value of 10.0 eV was used, for forsterite, 9.4 eV and for olivine, 9.7 eV.

2.4 Cut-off energy, E_C

The cut-off energy, E_C, is the energy below which trajectories of particles within the solid are no longer followed and is essentially a computational parameter chosen to moderate cpu usage. In the present work, all trajectories are followed down to an energy equal to that of the surface binding energy, E_S.

2.5 Grain density

A further parameter of the model is the density of the target material. FMFF showed that variations in the density of ±20 per cent caused variations in sputtering yields of no more than 5 per cent. Thus the density is not a critical parameter. Grains in the ISM remain cold during passage of a shock wave, and a temperature of 20 K has been taken to be representative (Flower & Pineau des Forêts 1995). Densities at 20 K were estimated by linear extrapolation of the values tabulated versus temperature for forsterite and fayalite (Anderson 1995) and found to be 3.25 ± 0.02 and 4.44 ± 0.02 g cm^{-3}, respectively, where the errors include those of extrapolation and the uncertainty in the dust temperature. Olivine at 20 K was assumed to have a density of the average of fayalite and forsterite, an assumption based on the principle that the lattice parameter, and hence crudely the density, of a solid solution is given by a mole-fraction-weighted mean of the substituents (sometimes known as 'Vegard's law'). The density of olivine used in the models was therefore 3.84 ± 0.02 g cm^{-3}. Room-temperature data for olivine show that Vegard's law is accurate to better than 3 per cent.

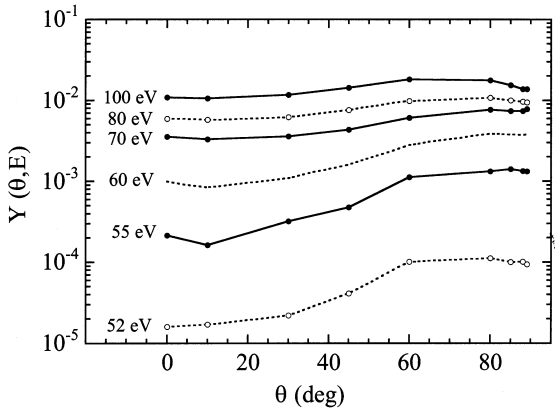

Figure 1. Variation of the sputtering yield, $Y(\theta, E)$, with the angle of incidence, θ, measured with respect to the normal to the surface and impact energy, E. The material is olivine and the case of the sputtering of Si following Si impact is considered.

2.6 Determination of the yields

As discussed in FMFF, the sputtering yield is a strong function of the angle of incidence of the impacting particle, with the highest yields associated with the more grazing angles of incidence. For example, the sputtering yield may change by one order of magnitude between normal incidence and grazing incidence. The behaviour at very grazing angles may be complicated and strongly energy dependent. This is illustrated in Fig. 1 for Si impacting on olivine. As in FMFF, care has been taken to ensure that the chosen angles and energies adequately sample this behaviour.

Collisions of particles with dust grains may be isotropic, or the projectiles may stream in one dimension, colliding with the grains, which are assumed to be spherical. FMFF examined both cases and showed that the computed yields were little different, especially at the lower energies of interest here. As in FMFF, we assume the isotropic case, which may arise if the dust grains are highly convolved and/or the grains are tumbling. The isotropic yield is given by

$$Y = \int_0^{\pi/2} \mathrm{d}\theta Y(\theta, E) \sin(\theta) \qquad (1)$$

where E is the impact energy and θ is the angle of incidence, measured with respect to the normal.

The accuracy of the values of sputtering yields depends on the inherent reliability of the techniques used in TRIM in the low-energy, low-yield regime and also on the uncertainties in the energies discussed above. Regarding the accuracy of TRIM, FMFF

showed that agreement between experimental and calculated yields was good down to impact energies of ≈200 eV. There are very few recent data below 1 keV impact energy with which to assess the accuracy of TRIM, and no advance can presently be made on the comparison made in FMFF. The sensitivity of the sputtering yields to the energies involved in sputtering was discussed in FMFF and is considered further in Section 3 below.

3 RESULTS OF CALCULATIONS OF SPUTTERING YIELDS

The results of our calculations of yields refer to a specific atom impacting on Mg_2SiO_4, Fe_2SiO_4 or $MgFeSiO_4$ (olivine) to yield a specific sputtered atom. The atoms studied – He, C, O, Si and Fe – cover the range of mass of astrophysically important species; H atoms carry too little momentum, at the differential velocities of gas and grains encountered in C-type shocks, to sputter significantly. Molecular species, such as CO and H_2O, also impact upon the grains. Data for the impact of atomic species may be used to estimate sputtering yields for molecules; this is discussed below.

Sputtering yields, Y, are collated in Tables 2–4 in the form of a three parameter (k, β, $E_{\rm th}$) fit

$$Y(E) = k \exp[-\beta/(E - E_{\rm th})], \quad (2)$$

where E is the impact energy and $E_{\rm th}$ may be interpreted as the sputtering threshold energy. This function (equation 2) is somewhat different from that used in FMFF; it was found to be more satisfactory for fitting the present data. By way of illustration, we plot in Fig. 2 the yield for the sputtering of Si from olivine ($MgFeSiO_4$), by O impact and Fe impact. The data points computed by TRIM and the fits to these data are given. For O impact, the functional form (2) is seen to yield an excellent representation of the data. For Fe impact, on the other hand, the fit is less good, although still adequate for the applications to be considered below. The fits illustrated in Fig. 2 may be considered to be representative of the best and worst cases.

Table 2. Parameters for use in equation (2) to calculate the sputtering yields of Mg_2SiO_4 (forsterite) for the impact of atoms in column A to yield the sputtered atoms in column B.

A	B	Mg_2SiO_4 $E_{\rm th}$ (eV)	k	β (eV)
He	Mg	$E \geqslant E_{\rm th} = 70$ eV	5.612e−2	65.925
	Si	$E \geqslant E_{\rm th} = 70$ eV	2.616e−2	64.940
	O	$E \geqslant E_{\rm th} = 70$ eV	1.085e−1	57.287
C	Mg	$E \geqslant E_{\rm th} = 45$ eV	1.502e−1	66.533
	Si	$E \geqslant E_{\rm th} = 45$ eV	7.041e−2	66.614
	O	$E \geqslant E_{\rm th} = 45$ eV	2.149e−1	53.613
O	Mg	$E \geqslant E_{\rm th} = 48$ eV	8.938e−2	36.988
	Si	$E \geqslant E_{\rm th} = 48$ eV	3.789e−2	35.813
	O	$E \geqslant E_{\rm th} = 48$ eV	1.257e−1	31.462
Si	Mg	$E \geqslant E_{\rm th} = 49$ eV	8.512e−2	27.917
	Si	$E \geqslant E_{\rm th} = 49$ eV	4.130e−2	27.171
	O	$E \geqslant E_{\rm th} = 49$ eV	1.258e−1	25.766
	O	$E \geqslant E_{\rm th} = 48$ eV	1.686e−1	34.626
Fe	Mg	$E \geqslant E_{\rm th} = 50$ eV	4.735e−2	71.750
	Si	$E \geqslant E_{\rm th} = 50$ eV	1.994e−2	68.964
	O	$E \geqslant E_{\rm th} = 50$ eV	9.273e−2	72.443

A more complete sample of the fits to the sputtering yields is to be seen in Fig. 3. Once again, the results are given for olivine, but for the complete range of impacting projectiles (He, C, O, Si and Fe) and for three different sputtered atoms (Mg, Si and Fe). The yield is plotted as a function of the velocity of impact, which can be related directly to the ion–neutral drift speed in the models discussed below. To compensate for their lower mass, He projectiles require higher velocities to induce sputtering than do the heavier species. Fig. 3 additionally shows that the sputtering efficiencies of heavier projectiles, such as Fe, may be less than

Table 3. Parameters for use in equation (2) to calculate the sputtering yields of Fe_2SiO_4 (fayalite) for the impact of atoms in column A to yield the sputtered atoms in column B.

A	B	Fe_2SiO_4 $E_{\rm th}$ (eV)	k	β (eV)
He	Fe	$E \geqslant E_{\rm th} = 74$ eV	1.587e−2	32.302
	Si	$E \geqslant E_{\rm th} = 74$ eV	7.879e−3	31.850
	O	$E \geqslant E_{\rm th} = 74$ eV	3.933e−2	28.465
C	Fe	$E \geqslant E_{\rm th} = 40$ eV	1.368e−1	93.337
	Si	$E \geqslant E_{\rm th} = 45$ eV	3.956e−2	55.012
	O	$E \geqslant E_{\rm th} = 45$ eV	1.447e−1	45.811
O	Fe	$E \geqslant E_{\rm th} = 40$ eV	1.289e−1	89.615
	Si	$E \geqslant E_{\rm th} = 45$ eV	4.035e−2	49.100
	O	$E \geqslant E_{\rm th} = 45$ eV	1.122e−1	40.541
Si	Fe	$E \geqslant E_{\rm th} = 45$ eV	1.486e−1	60.609
	Si	$E \geqslant E_{\rm th} = 45$ eV	3.207e−2	39.497
	O	$E \geqslant E_{\rm th} = 45$ eV	1.549e−1	55.622
Fe	Fe	$E \geqslant E_{\rm th} = 50$ eV	2.743e−2	17.041
	Si	$E \geqslant E_{\rm th} = 46$ eV	1.565e−2	44.459
	O	$E \geqslant E_{\rm th} = 44$ eV	9.229e−2	61.813

Table 4. Parameters for use in equation (2) to calculate the sputtering yields of $MgFeSiO_4$ (olivine) for the impact of atoms in column A to yield the sputtered atoms in column B.

A	B	$MgFeSiO_4$ $E_{\rm th}$ (eV)	k	β (eV)
He	Mg	$E \geqslant E_{\rm th} = 73$ eV	1.221e−2	41.187
	Fe	$E \geqslant E_{\rm th} = 73$ eV	1.151e−2	40.976
	Si	$E \geqslant E_{\rm th} = 73$ eV	1.224e−2	42.175
	O	$E \geqslant E_{\rm th} = 73$ eV	5.348e−2	36.030
C	Mg	$E \geqslant E_{\rm th} = 48$ eV	2.935e−2	36.740
	Fe	$E \geqslant E_{\rm th} = 47$ eV	2.386e−2	42.794
	Si	$E \geqslant E_{\rm th} = 48$ eV	2.698e−2	36.502
	O	$E \geqslant E_{\rm th} = 48$ eV	1.054e−1	30.812
O	Mg	$E \geqslant E_{\rm th} = 48$ eV	2.884e−2	30.238
	Fe	$E \geqslant E_{\rm th} = 44$ eV	4.116e−2	59.438
	Si	$E \geqslant E_{\rm th} = 47$ eV	3.373e−2	37.810
	O	$E \geqslant E_{\rm th} = 47$ eV	1.006e−1	31.588
Si	Mg	$E \geqslant E_{\rm th} = 48$ eV	2.093e−2	27.730
	Fe	$E \geqslant E_{\rm th} = 47$ eV	4.324e−2	42.335
	Si	$E \geqslant E_{\rm th} = 47$ eV	2.217e−2	28.013
	O	$E \geqslant E_{\rm th} = 46$ eV	1.149e−1	46.018
Fe	Mg	$E \geqslant E_{\rm th} = 47$ eV	1.119e−2	40.913
	Fe	$E \geqslant E_{\rm th} = 50$ eV	1.018e−2	12.328
	Si	$E \geqslant E_{\rm th} = 47$ eV	1.190e−2	42.624
	O	$E \geqslant E_{\rm th} = 44$ eV	8.657e−2	68.108

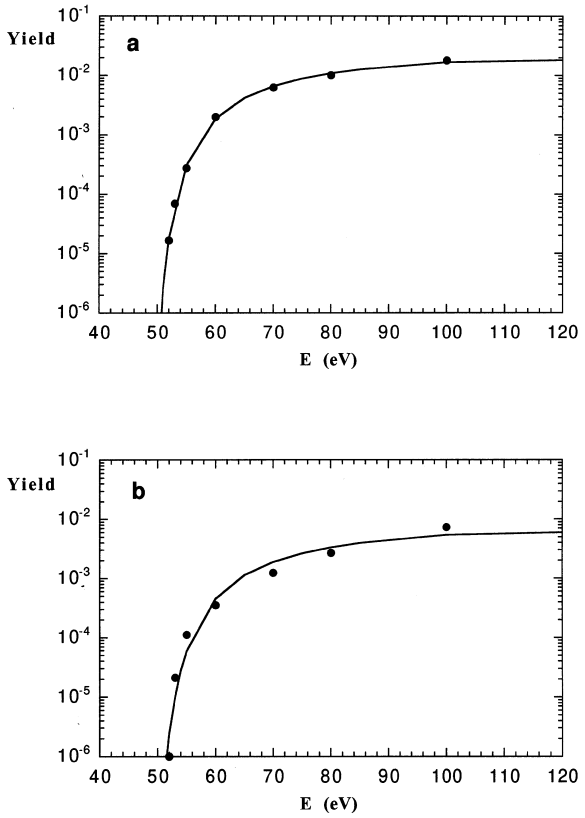

Figure 2. (a) The yield of Si sputtered from olivine by O impact. The points are the data obtained using TRIM and the curve is the fit (equation 2). (b) As in (a), but for Fe impact. The fits illustrated here may be considered representative of the best (a) and worst (b) cases.

those of lighter projectiles. For example Fig. 3(c) shows that, away from the threshold region, the sputtering yield of O or Si impacting on olivine to yield Fe is about 4 times greater than that associated with the impact of Fe.

We now consider the sensitivity of our results to uncertainties in the surface binding energy, the lattice binding energy, the density of the target and the displacement energy. Tests were conducted in the threshold region, where the sensitivity is greatest. Since our aim is to characterize the velocities of shocks, the uncertainty in the sputtering yield is expressed in terms of velocity. This procedure affords a clearer description of the sputtering threshold region, where a very large change in sputtering yield accompanies a small change in velocity (cf. Fig. 2).

Surface and lattice binding energies and the density of the target have been varied by ± 10 per cent in calculations involving sputtering of O atoms from fayalite by O atoms, for an impact velocity of $25\,\mathrm{km\,s^{-1}}$. The corresponding uncertainties in the velocity do not exceed approximately ± 0.25 per cent. However, our results are more sensitive to the value of the displacement energy. A variation in this energy from 45 to 55 eV, that is by ± 10 per cent, corresponds to an uncertainty in the velocity of approximately ± 6 per cent. Poor knowledge of the displacement energy is the single most important contributor to uncertainty in the sputtering yields reported in this paper. In Section 4, the velocities assigned to any computation should be accorded an error of ± 6 per cent.

The relationship between sputtering by atomic and molecular projectiles is deduced from the experimental work of Yao et al.

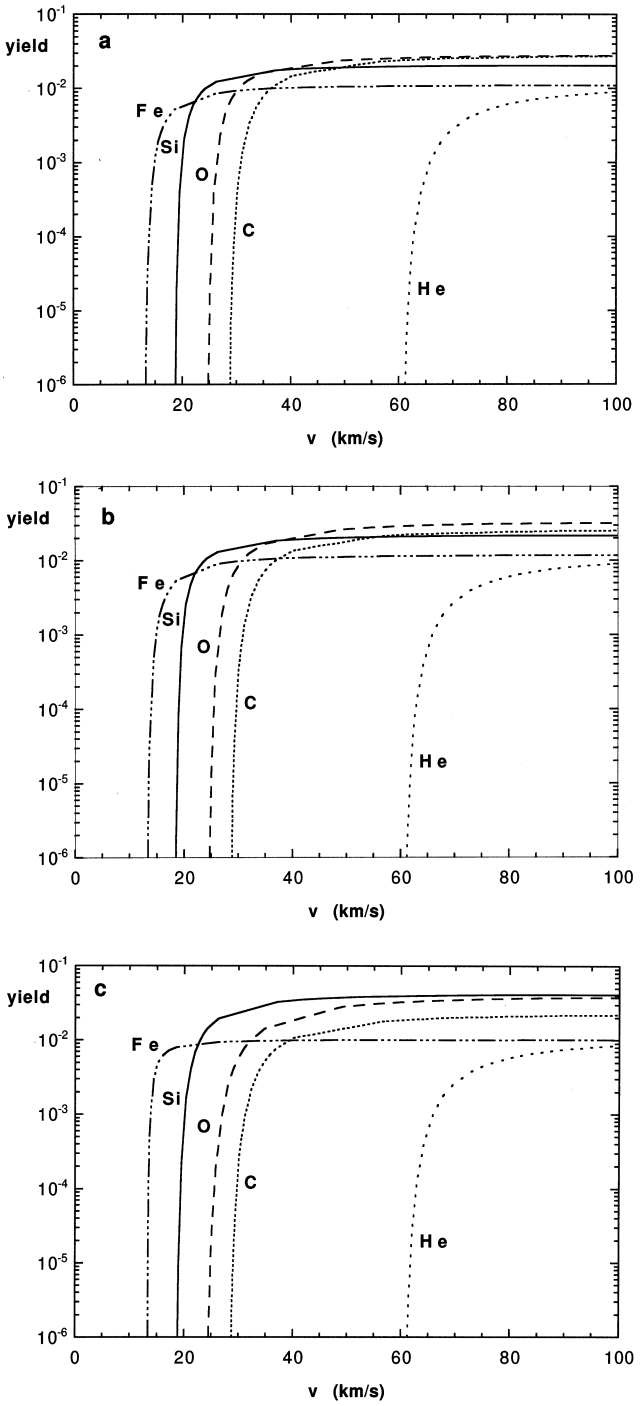

Figure 3. (a) The yield of Mg sputtered from olivine by the named projectiles. The curves are the fits (equation 2) to the TRIM data. (b) As in (a), but for sputtering of Si. (c) As in (a), but for sputtering of Fe.

(1998), the only authors to report sputtering yields for molecular impact at energies of less than 1 keV. At high energies, i.e. >1 keV, molecular sputtering yields correspond to the sum of the effects of the individual atoms in the molecule. However, from a comparison of yields of Au sputtered by N^+ and N_2^+, Yao et al. (1998) found a considerable enhancement of the yield near threshold, compared with the independent-atom model observed at high energies. Similar results were obtained for O^+ and O_2^+. It was found that, below a certain impact energy, molecules give rise

Table 5. Elemental fractions of Mg, Si and Fe sputtered from olivine and column densities, *N*, of atomic Si and of SiO, for the C-shock models with the specified velocity and pre-shock gas density. The initial magnetic induction was assumed to scale with the density as $B(\mu\mathrm{G}) = [n_\mathrm{H}(\mathrm{cm}^{-3})]^{1/2}$. Numbers in parentheses are powers of 10.

v_s (km s^{-1})	n_H (cm^{-3})	(Si)	(Mg)	(Fe)	N(Si) (cm^{-2})	N(SiO) (cm^{-2})
20	1.(04)	0	0	0	8.6(05)	1.9(07)
20	1.(05)	0	0	0	1.8(05)	1.1(06)
20	1.(06)	0	0	0	3.9(04)	1.3(05)
25	1.(04)	5.7(−04)	2.9(−04)	6.5(−04)	1.9(12)	7.5(13)
25	1.(05)	3.5(−04)	1.5(−04)	5.5(−04)	9.9(11)	4.5(13)
25	1.(06)	1.7(−04)	5.8(−05)	5.0(−04)	5.3(11)	2.1(13)
30	1.(04)	6.6(−02)	5.5(−02)	8.0(−02)	1.5(14)	7.8(15)
30	1.(05)	6.1(−02)	5.2(−02)	7.4(−02)	2.3(14)	8.0(15)
30	1.(06)	5.4(−02)	4.5(−02)	6.4(−02)	2.6(14)	7.0(15)
35	1.(04)	2.2(−01)	2.0(−01)	2.9(−01)	8.8(14)	2.4(16)
35	1.(05)	2.0(−01)	1.9(−01)	2.8(−01)	1.4(15)	2.5(16)
35	1.(06)	1.9(−01)	1.7(−01)	2.5(−01)	4.7(15)	1.8(16)
40	1.(04)	4.5(−01)	4.2(−01)	5.9(−01)	3.7(15)	4.8(16)
40	1.(05)	4.5(−01)	4.2(−01)	5.8(−01)	1.5(16)	4.3(16)
45	1.(04)	7.0(−01)	6.3(−01)	9.0(−01)	2.8(16)	5.4(16)
45	1.(05)	7.1(−01)	6.4(−01)	9.1(−01)	5.2(16)	4.1(16)

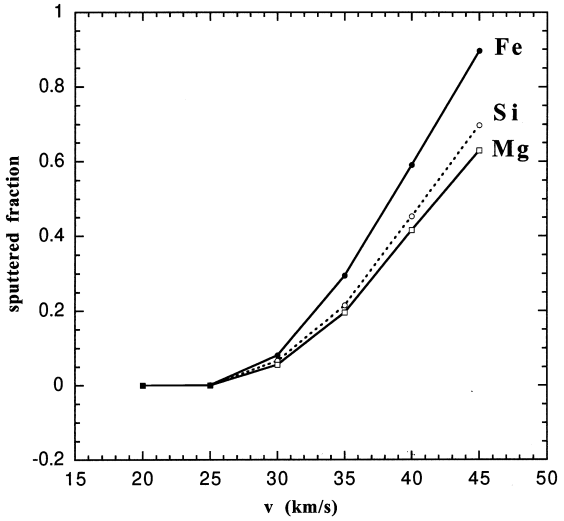

Figure 4. Sputtered fractions of Mg, Si and Fe, as functions of the C-shock speed. The pre-shock gas density is $n_\mathrm{H} = 10^4\,\mathrm{cm}^{-3}$ and the initial transverse magnetic induction is $B(\mu\mathrm{G}) = [n_\mathrm{H}(\mathrm{cm}^{-3})]^{1/2} = 100$.

to sputtering yields characteristic of particles of mass equal to the sum of the masses of the constituent atoms. Using the method outlined by Yao et al. (1998), involving the comparison of collision times with half-vibrational periods, we estimate that important molecular species, such as CO, H_2O, N_2 and O_2, tend towards behaving as particles of effective mass equal to the sum of the masses of their atomic constituents, at velocities of impact for CO below approximately $50\,\mathrm{km\,s}^{-1}$, for H_2O below 80–$90\,\mathrm{km\,s}^{-1}$, for N_2 below $50\,\mathrm{km\,s}^{-1}$ and for O_2 below $35\,\mathrm{km\,s}^{-1}$. Differential velocities, between charged grains and neutrals, in the C-type shocks considered below place the calculations in the threshold regime, where molecules sputter as atoms of equivalent mass. Thus, the sputter yields used for molecules were those computed for the atomic species (^{12}C, ^{16}O, ^{28}Si) the mass of which is closest to that of the impacting molecule. This procedure was also adopted by FMFF, although there was no supporting experimental evidence available at that time.

4 MODELS OF C-TYPE SHOCKS

Shocks propagating in interstellar molecular clouds are expected to have C-type characteristics owing to the decoupling of the flows of the charged and the neutral fluids. Charged grains undergo sputtering in collisions with the abundant neutral particles, principally molecules. As mentioned at the end of the previous section, we adopt the sputtering yield computed for the impacting atom of nearest mass.

The present model of a planar C-type shock is a development of that used by FMFF. We note that the dynamical and chemical rate equations are solved in parallel, thereby allowing for the variation in the fractional ionization of the gas owing to chemical reactions within the shock wave. In addition to the ion–neutral drag, the collisional coupling between the neutral gas and the charged grains is included. More information may be found in Flower & Pineau des Forêts (1999). When incorporating the new sputtering yields, discussed above, we make allowance for the variation of the radius of the grain core as material is removed by the sputtering process; the method employed is described in Appendix A.

We have computed a grid of models for pre-shock densities in the range $10^4 \leqslant n_\mathrm{H} = n(\mathrm{H}) + 2n(\mathrm{H_2}) \leqslant 10^6\,\mathrm{cm}^{-3}$ and shock speeds $20 \leqslant v_s \leqslant 45\,\mathrm{km\,s}^{-1}$. The initial value of the transverse magnetic induction was given by the frequently used scaling relation $B(\mu\mathrm{G}) = [n_\mathrm{H}(\mathrm{cm}^{-3})]^{1/2}$ (Troland & Heiles 1986). It was assumed that elemental Mg, Si and Fe were initially in the form of olivine, $MgFeSiO_4$, with a trace amount (10^{-3} of the elemental abundance) of Fe in the gas phase, as a representative heavy

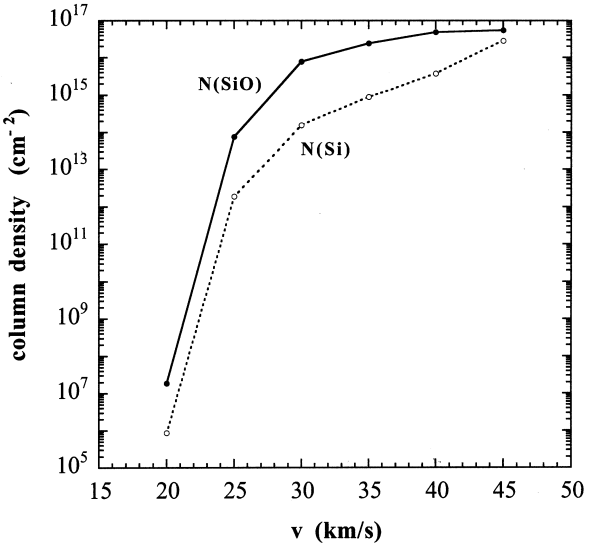

Figure 5. Column densities of atomic Si and SiO, as functions of the C-shock speed. The pre-shock gas density is $n_H = 10^4\,cm^{-3}$ and the initial transverse magnetic induction is $B(\mu G) = [n_H(cm^{-3})]^{1/2} = 100$.

Table 6. Elemental fractions of Mg, Si and Fe sputtered from olivine, fayalite and forsterite for a C-shock model with $v_s = 30\,km\,s^{-1}$, $n_H = 10^4 cm^{-3}$ and $B = 100\,\mu G$. Numbers in parentheses are powers of 10.

	[Si]	[Mg]	[Fe]
$MgFeSiO_4$	6.6(−02)	5.5(−02)	8.0(−02)
Fe_2SiO_4	6.7(−02)		1.6(−01)
Mg_2SiO_4	1.1(−01)	2.1(−01)	

metal. We followed the chemical processing of silicon released into the gas phase (see Schilke et al. 1997), but the gas-phase chemistry of magnesium and iron have not yet been included in the model.

In Table 5, we summarize the results obtained for the sputtered species. For each model are given the fractions of the initially solid Mg, Si and Fe which are released into the gas phase. Also listed are the column densities of atomic Si and of SiO, computed within the shock wave by integrating along its direction of propagation. It may be seen that, when the sputtered fractions are significant, for $v_s > 25\,km\,s^{-1}$, their values are insensitive to the pre-shock gas density. In Fig. 4, we show the variations with the shock speed of the sputtered fractions. Evident is the knee in the curves, where the ion–neutral drift velocity becomes sufficiently large to induce sputtering. More than 90 per cent of the Fe, 70 per cent of the Si and 60 per cent of the Mg are removed by sputtering when $v_s = 45\,km\,s^{-1}$. By extrapolation, we deduce that the grains would be essentially completely destroyed for v_s in excess of $50\,km\,s^{-1}$. However, as TRIM makes no allowance for the effects of prior exposure to ion impact, notably ion implantation, the quantitative aspects of this conclusion should be viewed with some caution.

The column densities of atomic Si and of SiO are plotted as functions of v_s in Fig. 5, for $n_H = 10^4\,cm^{-3}$. Large column densities of SiO, approaching $10^{17}\,cm^{-2}$, are obtained for the highest shock speeds. Such values are much in excess of the column densities of SiO observed in molecular outflows, that are typically $N(SiO) \leqslant 10^{15}\,cm^{-2}$ (cf. FMFF; Schilke et al. 1997). Part of the discrepancy may be attributable to beam dilution. However, it is clear that the assumption of a planar stationary state C-type shock is unrealistic, given the geometries and the time-scales which are relevant to molecular outflows. Models of bow shocks or non-stationary shocks (Flower & Pineau des Forêts 1999; Wilgenbus et al. 2000) are expected to yield lower column densities.

In Table 6 we compare the elemental fractions sputtered from olivine, fayalite (Fe_2SiO_4) and forsterite (Mg_2SiO_4), for $v_s = 30\,km\,s^{-1}$ and $n_H = 10^4\,cm^{-3}$. The variations with the chemical composition of the grains reflect the relative magnitudes of the sputtering yields, particularly as they approach saturation.

5 CONCLUDING REMARKS

The sputtering yields reported here were derived using techniques that are well established in the areas of microelectronic device fabrication and solid-state chemistry. Our data serve to remove a significant source of error in calculations of sputtering following the fast impact of a variety of species on olivine and related silicate grains. The computed sputtering yields are subject to some remaining uncertainties, but these are well defined and have been reduced, so far as is currently possible, by a critical evaluation of the energetics of the sputtering process.

The high yields of Si, for example, computed for moderate impact velocities have important implications for the nature of C-type shocks. As we have noted above, observations constrain the column density of SiO to be typically $\leqslant 10^{15}\,cm^{-2}$. For the planar C-type shocks considered here, this column density would imply shock velocities in a narrow range between approximately 25 and $30\,km\,s^{-1}$, independent of the pre-shock gas density. Such a restriction on the range of the shock velocities appears to be unphysical, unless there is an as yet unknown mechanism that prevents the velocities of C-type shocks from exceeding approximately $30\,km\,s^{-1}$. Our results suggest that geometries other than planar or non-stationary shocks need to be considered when modelling fast outflows in regions of star formation.

ACKNOWLEDGMENTS

We should like to thank H. Mutschke of the University of Jena, Germany, for supplying us with a room-temperature value of the density of olivine. We are grateful to W. Eckstein of the Max-Planck Insitut für Plasmaphysik, Garching, Germany, for his help in interpreting some of our sputtering results.

REFERENCES

Anderson O. L., 1995, Equations of State of Solids for Geophysics and Ceramic Science, OUP, New York
Catlow C. R. A., Mackrodt W. C., 1982, in Catlow C. R. A., Mackrodt W. C., eds, Computer Simulation of Solids. Springer-Verlag, Berlin
Dick B. G., Overhauser A. W., 1958, Phys. Rev., 112, 90
Dickens P. G., Heckingbottom R., Linnett J. W., 1968, Trans. Faraday Soc., 64, 1489
Dutrey A., Guilloteau S., Bachiller R., 1997, A&A, 325, 758
Eckstein W., 1991, Computer Simulations of Ion–Solid Interactions. Springer-Verlag, Berlin
Field D., May P. W., Pineau des Forêts G., Flower D. R., 1997, MNRAS, 285, 839 (FMFF)
Flower D. R., Pineau des Forêts G., 1995, MNRAS, 275, 1049
Flower D. R., Pineau des Forêts G., 1999, MNRAS, 308, 271

Hayes W., Stoneham A. M., 1985, Defect and Defect Processes in Non-Metallic Solids. Wiley, New York
Lefloch B., Castets A., Cernicharo J., Loinard L., 1998, ApJ, 504, L109
Lewis G. V., Catlow C. R. A., 1985, J. Phys. C: Solid State Phys., 18, 1149
Lidiard A. B., Norgett M. J., 1972, in Herman F., Dalton W. W., Koeler T. R., eds, Computational Solid State Physics. Plenum, New York, p. 385
Mott N. F., Littleton M. T., 1938, Trans. Faraday Soc., 34, 485
Mackrodt W. C., Stewart R. F., 1979, J. Phys. C, 12, 431
Patel A., Price G. D., Mendelssohn M., 1991, Phys. Chem. Minerals, 17, 690
Pirronello V., 1993, in Millar T. J., Williams D. A., eds, Dust and Chemistry in Astronomy. IOP Publishing, Bristol
Purton J. A., Allan N. L., Blundy J. D., Wassermanm E. A., 1996, Geochim. Cosmochim. Acta, 60, 4977
Purton J. A., Allan N. L., Blundy J. D., 1997a, J. Mater. Chem., 7, 1947
Purton J. A., Allan N. L., Blundy J. D., 1997b, Geochim. Cosmochim. Acta, 61, 3927
Sanders M. J., Leslie M., Catlow C. R. A., 1984, J. Chem. Soc., Chem. Commun., 1271
Schilke P., Walmsley C. M., Flower D. R., Pineau des Forêts G., 1997, A&A, 321, 293
Taylor M. B., Barrera G. D., Allan N. L., Barron T. H. K., 1997, Phys. Rev. B, 56, 14380
Troland T. H., Heiles C., 1986, ApJ, 301, 339
Wilgenbus D., Cabrit S., Pineau des Forêts G., Flower D. R., 2000, A&A, 356, 1010
Winkler B., Dove M. T., Leslie M., 1991, Amer. Miner., 76, 313
Yao Y. et al., 1998, Phys. Rev. Lett., 81, 550
Ziegler J. F., Biersack J. P., Littmark U., 1985, The Stopping and Range of Ions in Solids. Pergamon, New York

APPENDIX A

We define ρ_g as the mass and n_g as the number of grains, per unit volume of the gas. The grains which undergo sputtering, in collisions with neutrals, are assumed to move with the velocity of the ionized fluid, v_i. In a stationary state,

$$\frac{d}{dz}(\rho_g v_i) = S_g, \tag{A1}$$

where S_g is the net rate of creation of grain mass, per unit volume of gas, arising from the competition between accretion and sputtering processes and z is the position coordinate (the shock is planar). Hence,

$$\frac{d}{dz}\ln \rho_g = \frac{S_g}{\rho_g v_i} - \frac{d}{dz}\ln v_i. \tag{A2}$$

Denoting the mean radius of the grains by a and the density of the grain material by ρ, we have

$$\rho_g = \frac{4}{3}\pi a^3 \rho n_g, \tag{A3}$$

or

$$\frac{d}{dz}\ln a = \frac{1}{3}\left(\frac{d}{dz}\ln \rho_g - \frac{d}{dz}\ln n_g\right) = \frac{1}{3}\left(\frac{d}{dz}\ln \rho_g + \frac{d}{dz}\ln v_i\right), \tag{A4}$$

as the flux of grains, $n_g v_i$, is assumed to be constant. Equations (A2) and (A4) are solved in parallel with the magnetohydrodynamical (MHD) and chemical rate equations. The mean radius, $a(z)$, is used to determine the geometrical cross-section of the grains, required in the determination of the sputtering (and accretion) rates (Flower & Pineau des Forêts 1995).

This paper has been typeset from a TEX/LATEX file prepared by the author.